

Toward Phase-Recovery Optical Nanoscopes

Sueli Skinner-Ramos^{1,2}, Hira Farooq¹, Hawra Alghasham¹ and Luis Grave de Peralta^{1,2}

1. Department of Physics and Astronomy, Texas Tech University, Lubbock, TX 79409, USA

2. Nano Tech Center, Texas Tech University, Lubbock, TX 79409, USA

Abstract: We discuss how recent advances in phase-recovery imaging techniques in combination with plasmonic UTSSs (ultrathin condensers) with a semiconductor substrate have paved the way for the development of novel optical nanoscopes. These optical nanoscopes are capable of imaging the intensity and the phase of the electric field distribution at the sample's plane.

Key words: Microscopy, nanoscopes, image formation theory, illumination design.

1. Introduction

For a long time, the Rayleigh resolution limit $\sim \lambda/(2NA_0)$, where λ is the wavelength of the light used for imaging and NA_0 is the numerical aperture of the objective lens, was considered to be the ultimate resolution limit of optical microscopes [1-4]. Since objective lenses have $NA_0 < 2$, imaging nanostructures with a size smaller than 100 nm using visible light was thought to be impossible. Nevertheless, the nanoimaging needs in subcellular biology and nanotechnology motivated further research in possible ways to overcome the resolution limitation of common optical microscopes. Advances in near-field imaging resulted in the first breakthrough with the development of NSOMs (near-field scanning optical microscopes) capable of imaging nanostructures [5]. The success of NSOMs encouraged the quest for far-field optical imaging techniques capable of resolving nanostructures, which recently added to the development of, not one, but several far-field optical nanoscopy techniques and a Nobel Prize recognizing the pioneers in this emerging field [6-11]. What was once considered the ultimate resolution limit of optical microscopes is today understood to be the best resolution possible for an image formed directly in a camera attached to a microscope. Existing optical

nanoscopy techniques circumvent the Rayleigh resolution limit by numerically reconstructing a nanoresolution image from multiple measured events. In NSOMs each measurement event corresponds to the electric field intensity at a different point of the sample [5], while in far-field optical nanoscopy techniques each measurement event is a low-resolution image containing partial [6-8] or indirect [9-11] information of the sample.

Like common optical microscopes, but with better resolution, existing optical nanoscopes permit imaging of the intensity distribution of the electric field in the sample's plane; however, they do not allow imaging of its phase distribution. This is a second limitation of any image formed directly on a camera that is only sensitive to the intensity of the light [1, 2, 12]. Numerous optical microscopy techniques have been developed to overcome this second limitation of common optical microscopes [13-28]; however, none of the existing optical nanoscopy techniques permits imaging of the phase distribution of the electric field at the sample's plane. In this work we present a feasible route for the realization of the first optical nanoscope capable of imaging both the intensity and phase distributions of the electric field at the sample's plane. Here we discuss how a PRON (phase-recovery optical nanoscope) could be built using a combination of a common optical microscope and a plasmonic UTC (ultrathin condenser) [29, 30]. The UTC is

Corresponding author: Luis Grave de Peralta, Ph. D., associate professor, research fields: physics, optics.

specially designed to allow collection of several far-field images of the sample formed directly in a camera, which are then numerically processed using either the FPM (Fourier ptychographic microscopy) [24-26] or the DSM (dual-space microscopy) phase-recovery algorithm [27, 28]. The rest of this paper is organized in the following manner: In Section 2 we discuss how the inclined illumination provided by a plasmonic UTC permits improving of the resolution of the image formed directly in the microscope's camera. We also discuss the limitations of this simple method for increasing the image resolution. In Section 3, we discuss how IDM (illumination-direction multiplexing) FPM and DSM allow for increasing the resolution of a microscope-UTC combination from $\sim\lambda/(2NA_o)$ to $\sim\lambda/(NA_o+NA_c)$ [31-33], where NA_c is the numerical aperture of the condenser. Here, for the first time, we report simulation results obtained using IDM-DSM. We also discuss the limitations of these numerical methods for increasing the image resolution and obtaining the phase-distribution of the electric field at the sample's plane. In addition, we present simulation results suggesting that a plasmonic UTC with a GaP substrate may have $NA_c \sim 10$ and therefore, combined with the IDM-FPM or IDM-DSM phase-recovery techniques, may result in numerically reconstructed intensity and phase images with nanoresolution. Finally, the conclusions of this work are presented in Section 4.

2. Plasmonic UTCs

The resolution limit of a common optical microscope using an illumination source producing a collimated beam of incident light perpendicular to the sample under observation is $\sim\lambda/NA_o$ [1-4]. By illuminating a periodic structure with the inclined illumination produced by a microscope condenser with $NA_c < NA_o$, the minimum period observable (p_{\min}) is reduced to $p_{\min} \sim \lambda/(NA_o+NA_c)$ [3, 4, 29, 30], which equals the Rayleigh resolution limit when $NA_c = NA_o$.

However, as illustrated in Fig. 1, it is not possible to obtain an image of a periodic structure with period (p) formed directly in a camera when $NA_c > NA_o$ and $\lambda/(NA_o+NA_c) > p < \lambda/(2NA_o)$; i.e., it is not possible to indefinitely improve the resolution of the microscope-condenser arrangement by simply increasing NA_c . Figs. 1a-1d show images of a plasmonic crystal with $p = 300$ nm formed directly in the CCD cameras placed at the RP (real plane) and FP (Fourier plane) of the experimental microscope-UTC setup, which is sketched in Fig. 1e and has been previously described in detail [29, 30, 34, 35]. In short, the source of inclined illumination was a plasmonic UTC with $NA_c \sim 1.1$ [29, 30, 34], whose transversal structure is sketched in the inset of Fig. 1e. The UTC is

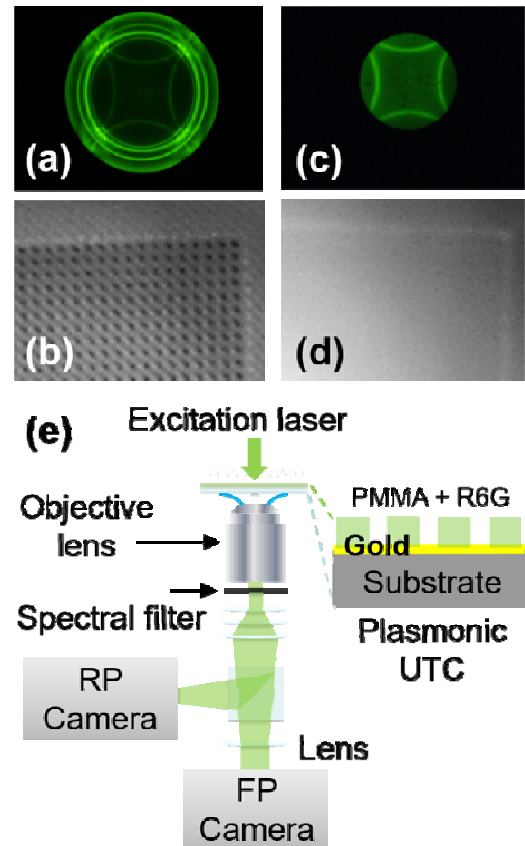


Fig. 1 (a), (c): FP; (b), (d): RP images of a photonic crystal with $p = 300$ nm obtained using a plasmonic UTC with $NA_c \sim 1.1$ and a microscope objective lens with $NA_c =$ (a-b) 1.3 and (c-d) 0.9; (e) Schematic illustration of microscope-UTC setup. The structure of the imaged plasmonic crystal is sketched in the inset of the Fig. 1e.

comprised of a ~ 150 μm glass substrate covered with a (thermally evaporated) 45 nm thick gold layer and coated with a ~ 110 nm thick layer of poly methyl methacrylate doped with Rhodamine-6G (PMMA-R6G). A 2 nm thick Cr layer was added in between the glass substrate and gold layer to promote adhesion. As sketched in the inset of Fig. 1e, the imaged photonic crystal was defined by patterning an array of air holes with square symmetry on top of the PMMA-R6G layer of the plasmonic UTC. A Nikon Eclipse Ti inverted microscope was fitted with two CCD (charge-coupled device) cameras to acquire RP and FP images. A high numerical aperture ($NA_o = 1.49$) oil-immersion objective lens, and a low numerical aperture ($NA_o = 0.9$) air objective lens, both with $100\times$ magnification were used, for collection and focusing, respectively. A 532 nm wavelength laser source was used to illuminate the sample from the top through the focusing objective. The laser excites the Rhodamine in the doped PMMA layer which in turn excites the SPPs (surface plasmon polaritons) at the gold/PMMA interface [36, 37]. Light coupled to SPPs subsequently leaks toward the glass substrate which sits above the collection objective lens [34, 36, 38]. A $\lambda = 570$ nm wavelength band-pass filter with a bandwidth of $\Delta\lambda = 10$ nm was placed after the objective lens to spectrally filter the leaked and transmitted radiation such that only light originating from the fluorescence/SPP leakage radiation was detected. The CCD cameras were then used to collect FP and RP images corresponding to the SPP leakage radiation [29, 30, 34, 35, 38]. The FP and RP images shown in Figs. 1a and 1b, respectively, were obtained with an objective lens having $NA_o = 1.49$, which corresponds to $\lambda/NA_o \sim 382$ nm $> p = 300$ nm. In excellent agreement, the array of air holes was not visible when the plasmonic crystal was under perpendicular illumination (not shown). However, the periodic structure of the plasmonic crystal is clearly visible in the RP image shown in Fig. 1b. This is a result of an improvement in resolution from λ/NA_o to $\lambda/(NA_o+NA_c) \sim 219$ nm $< p$ resulting by

illuminating the sample with the inclined illumination produced by the plasmonic UTC with $NA_c < NA_o$. The resolution of the plasmonic crystal structure in the RP image shown in Fig. 1b is in excellent correspondence with the presence of two consecutive diffraction features in the FP image shown in Fig. 1a [12]. A centered, bright, zero-order diffraction ring with radius ~ 1.1 NA units is clearly visible in Fig. 1a. In addition, 4 arcs with the same square symmetry of the plasmonic crystal, which corresponds to the first-order diffraction rings, are also visible in Fig. 1a. The presence of rings in the FP images is a signature of the illumination produced by plasmonic UTCs [29, 30, 39]. There are also 4 arcs in the FP image shown in Fig. 1c. However, the zero-order diffraction ring was not captured by the objective lens with $NA_o = 0.9 < NA_c = 1.1$ that was used for obtaining the FP and RP images shown in Figs. 1c and 1d, respectively. Consequently, the periodic structure of the plasmonic crystal cannot be seen in the RP image shown in Fig. 1d, which is also in agreement with $p < \lambda/(2NA_o) \sim 317$ nm when evaluated for $NA_o = 0.9$. It is worth noting that in this case $\lambda/(NA_o+NA_c) \sim 285$ nm $< p < \lambda/(2NA_o)$ but the periodic structure could not be recorded directly because $NA_c > NA_o$. This illustrates that the resolution limit of any image formed directly in the RP of a microscope-condenser combination can only be improved, up to the Rayleigh resolution limit, by increasing NA_c from 0 (perpendicular illumination) up to $NA_c = NA_o$. Any additional increment of NA_c above the NA_o value fails to increase the resolution of the image directly formed in the camera.

3. Illumination Direction Multiplexing FPM and DSM Using Plasmonic UTCs

When $NA_c > NA_o$ and $\lambda/(NA_o+NA_c) > \lambda/(2n)$, where (n) is the refractive index of the medium surrounding the sample, phase-recovery imaging techniques like FPM and DSM can be used to obtain a numerically-reconstructed high-resolution image with a resolution $\sim \lambda/(NA_o+NA_c) < \lambda/(2NA_o)$ [23, 24, 27, 28].

The details of the condition $\lambda/(NA_o+NA_c) > \lambda/(2n)$ will be discussed in detail below, for now we will assume that it is fulfilled. Originally, FPM and DSM were developed assuming that the sample is successively illuminated from numerous directions, a single direction at a time. In FPM [23-26] and DSM [27, 28], a low-resolution RP image and an FP-RP image pair is directly recorded in a microscope's camera for each direction, respectively. The set of experimental images are then numerically processed using a phase-recovery algorithm [23-28]. As a result, a synthetic FP image with a large numerical aperture $NA_s = NA_o + NA_c$, and the intensity and phase distributions of the electric field at the sample's plane with a resolution $\sim \lambda/NA_s$ are numerically obtained [23-28]. FPM has also been extended to the case where the sample is illuminated simultaneously from different directions (IDM) [31-33]. This is important for our purposes because plasmonic UTCs illuminate the sample simultaneously from every direction, forming a hollow cone, whose intersection with the microscope's FP is a ring [39]. In Fig. 2 and below, we present the IDM-DSM phase-recovery algorithm for the first time.

The IDM-DSM algorithm combines the principal

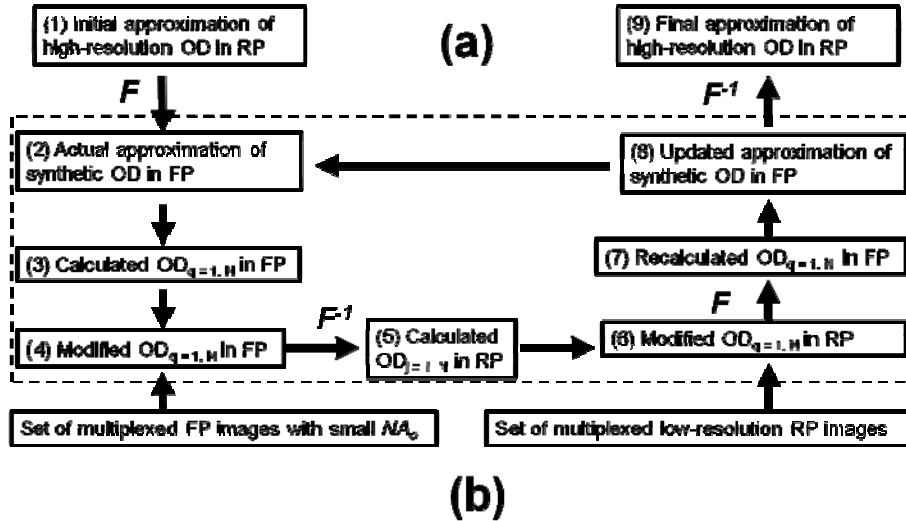
ideas behind the IDM-FPM [31-33] and DSM algorithms [27, 28]. As shown in block (1) of Fig. 2a the IDM-DSM algorithm starts (iteration index $m = 0$) by assuming an arbitrary amplitude ($a_{m=0}(r)$) and phase ($p_{m=0}(r)$) for arbitrary OD (optical disturbance) at the microscope's RP, ($a(r)\exp(ip(r))$). Then, as shown in block (2) of Fig. 2a the initial approximation ($m = 1, j = 1$) for the actual OD at the microscope's FP is obtained by applying a 2D (two-dimensional) FT operation to the initial OD in the following way:

$$A_{m=1,j=1}^{act}(k)e^{ip_{m=1,j=1}^{act}(k)} = F[a_{m=0}(r)e^{ip_{m=0}(r)}]. \quad (1)$$

Then, as sketched in block (3) in Fig. 2a, the ODs associated to each of the single illumination directions (labeled $q = 1, 2, \dots, N$), which contribute to the first ($j = 1$) multiplexed low-resolution RP image, are calculated as shown:

$$A_{m,j,q}(k)e^{ip_{m,j,q}(k)} = A_{m,j}^{act}(k-k_q)e^{ip_{m,j}^{act}(k-k_q)} \cdot W_0, \quad q=1,2,\dots,N(2)$$

where W_0 is a circular window of radius NA_o and centered at $k = 0$. Eq. (2) corresponds to the successive application of the operations "shift" and "window." First, the complex function describing the optical disturbance in the Fourier plane (FP-OD) is



$$\text{Modified } A(OD_q) = \sqrt{I_q - \frac{I_q}{I_T} \sum_{k \neq q} [A(OD_k)]^2}, \quad I_T = \sum_{k=1}^N [A(OD_k)]^2$$

Fig. 2 Flow diagram of the IDM-DSM phase-recovery algorithm.

shifted toward k_q , the FP position corresponding to the q^{th} illumination direction. The shift is then followed by a multiplication by the circular window parameter W_o , so that the resulting FP image is limited to an experimentally realizable numerical aperture (NA_o). As sketched in block (6) in Figs. 2a and 2b, in the IDM-DSM algorithm, the amplitude of the calculated FP-ODs is modified as shown:

$$A_{m,j,q}^{\text{mod}}(r) = \sqrt{\frac{I_{FP,j}}{I_{FPT,j}}} A_{m,j,q}(r), \quad (3)$$

$$I_{FPT,j} = \sum_{q=1}^N I_{FP,j,q}, \quad I_{FP,j,q} = [A_{m,j,q}(r)]^2.$$

where $I_{FP,j}$ is the intensity of the experimental (or simulated) multiplexed low-resolution RP image number j . This is in contrast to single illumination-direction DSM, where the amplitude of the calculated FP-OD ($a_{m,j,q}(r)$) is instead substituted by the square root of the intensity of the corresponding experimental (or simulated) low-resolution FP image [27, 28]. The incoherent superposition condition, which requires that the sum of all modified intensities ($I_{\text{modFP},j,q}$) contributing to the formation of the multiplexed low-resolution FP image number j should be equal to $I_{FP,j}$. This prompts us to rewrite the equivalent expression of Eq. (3) for an incoherent source as:

$$\sum_{q=1}^N I_{\text{modFP},j,q} = I_{FP,j}, \quad (4)$$

$$I_{\text{modFP},j,q} = [A_{m,j,q}^{\text{mod}}(r)]^2 = \frac{I_{FP,j}}{I_{FPT,j}} \sum_{l \neq q} I_{FP,j,l}.$$

As sketched in block (5) in Fig. 2a, the ODs in the RP (RP-ODs) corresponding to each modified FP-OD are then obtained by applying an inverse 2D Fourier transform (F^{-1}) operation as follows:

$$a_{m,j,q}(r) e^{ip_{m,j,q}(r)} = F^{-1} \left[A_{m,j,q}^{\text{mod}} e^{ip_{m,j,q}(k)} \right], \quad q=1,2,\dots,N \quad (5)$$

As sketched in block (5) in Figs. 2a and 2b, like in IDM-FPM, in the IDM-DSM algorithm, the amplitude of the calculated RP-ODs is modified in the following way [31-33]:

$$a_{m,j,q}^{\text{mod}}(r) = \sqrt{\frac{I_{RP,j}}{I_{RPT,j}}} a_{m,j,q}(r), \quad (6)$$

$$I_{RPT,j} = \sum_{q=1}^N I_{RP,j,q}, \quad I_{RP,j,q} = [a_{m,j,q}(r)]^2.$$

where $I_{RP,j}$ is the intensity of the experimental (or simulated) multiplexed low-resolution RP image number j . Again, this is in contrast to single illumination-direction DSM, where the amplitude of the calculated RP-OD ($a_{m,j,q}(r)$) is instead substituted by the square root of the intensity of the corresponding experimental (or simulated) low-resolution RP image [27, 28]. Eq. (6) must be modified to fulfill the incoherent superposition condition, that requires that the sum of all modified intensities ($I_{\text{modRP},j,q}$) contributing to the formation of the multiplexed low-resolution RP image number j should be equal to $I_{RP,j}$, as follows:

$$\sum_{q=1}^N I_{\text{modRP},j,q} = I_{RP,j}, \quad (7)$$

$$I_{\text{modRP},j,q} = [a_{m,j,q}^{\text{mod}}(r)]^2 = \frac{I_{RP,j}}{I_{RPT,j}} \sum_{l \neq q} I_{RP,j,l}.$$

As sketched in block (7) in Fig. 2a, the FP-ODs corresponding to each modified RP-OD are recalculated with the following equation:

$$A_{m,j,q}^{\text{rec}}(k) e^{ip_{m,j,q}^{\text{rec}}(k)} = F \left[a_{m,j,q}^{\text{mod}}(r) e^{ip_{m,j,q}(r)} \right] \cdot W_o. \quad (8)$$

It is worth noting that the recalculated FP-ODs (block (7) in Fig. 2a) are improved versions of the previously calculated FP-ODs (block (3) in Fig. 2a) because the information contained in the experimental (or simulated) multiplexed images has been incorporated to the recalculated FP-ODs. Then, as sketched in the block (8) of Fig. 2a, the next approximation of the synthetic FP-OD is calculated in the following way:

$$A_{m,j}^{\text{upd}}(k) e^{ip_{m,j}^{\text{upd}}(k)} = A_{m,j}^{\text{act}}(k) e^{ip_{m,j}^{\text{act}}(k)} + \alpha \sum_{q=1}^N \left[\gamma A_{m,j,q}^{\text{rec}}(k+k_q) e^{ip_{m,j,q}^{\text{rec}}(k+k_q)} - \beta A_{m,j,q}(k+k_q) e^{ip_{m,j,q}(k+k_q)} \right]. \quad (9)$$

As shown by arrow between blocks (8) and (2) in Fig. 2a, after the synthetic FP-OD is updated, it is

used as the actual approximation for the next set of multiplexed images ($j = 2, 3 \dots, M$). The operations included in the box with discontinuous-line in Fig. 2a are successively done for each pair of experimental (or simulated) multiplexed low-resolution RP and FP images. The “round-trip” application of steps outlined in blocks (2)-(8) constitutes the first algorithm iteration ($m = 1$). The algorithm should converge after several iterations. Finally, as shown in the block (9) in Fig. 2a, the amplitude and phase corresponding to the final high-resolution RP image is obtained by applying an inverse 2D Fourier transform of the complex function corresponding to the updated FP-OD. We conducted IDM-DSM simulations setting $p(r)=0$ and $a(r)$ equal to the square root of the intensity corresponding to the first multiplexed low-resolution RP image used in the algorithm as the initial approximation of the RP-OD. We assumed a set of 64 illumination directions, each direction corresponding to an LED in a previously reported hemispherical digital condenser [27, 28, 33]. The HDC is formed by 4 ring-like rows with numerical aperture values of $NA_c = 0.57, 0.73, 0.89, 0.97$. Each row contains 16 uniformly distributed LEDs. Light emitted by four consecutive LEDs in the same HDC’s

row was multiplexed in each of the 16 pairs of simulated multiplexed RP-FP images. Fig. 3 shows simulation results corresponding to a photonic crystal with rectangular symmetry and two different periods $p_x = 800$ nm and $p_y = 340$ nm, which were obtained using the IDM-DSM phase recovery algorithm described in Fig. 2. Figs. 3a and 3b show an example of simulated multiplexed RP and FP images corresponding to $NA_o = 0.8$, $NA_c = 0.73$, and a $\lambda = 570$ nm wavelength of the light used for imaging. In the low-resolution multiplexed RP image shown in Fig. 3a, a periodic structure corresponding to the largest period of the sample, $p_x = 800$ nm, is clearly visible; however, the smallest period ($p_y = 340$ nm) is invisible. This is in excellent correspondence with $p_x > \lambda/(NA_o+NA_c) \sim 373$ nm but $p_y < \lambda/(2NA_o) \sim 356$ nm. In the simulated multiplexed FP image shown in Fig. 3b, four relatively bright spots are clearly visible inside of a disk of radius equal to $NA_o=0.8$. Each spot in Fig 3b correspond to the zero-order diffraction spot associated with the light produced by one of the four multiplexed LEDs with $NA_c = 0.73 < NA_o$. Figs. 3c and 3d show the high-resolution intensity and phase distributions numerically calculated using the IDM-DSM phase-recovery algorithm described above.

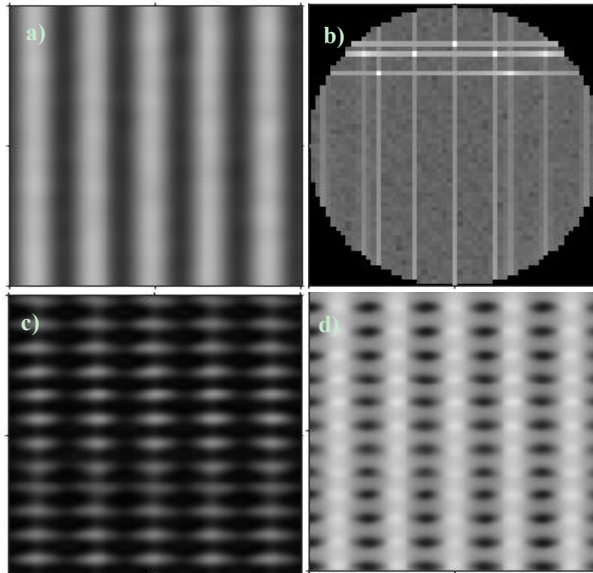


Fig. 3 Simulated multiplexed (a) RP and (b) FP images of a photonic crystal with rectangular symmetry, $p_x = 800$ nm, and $p_y = 340$ nm obtained using $\lambda = 570$ nm, $NA_o \sim 0.8$ and $NA_c = 0.73$. High-resolution (c) intensity and (d) phase distributions obtained using the IDM-DSM phase-recovery algorithm after 10 iterations.

Both sample periodicities are clearly seen in both images demonstrating the improvement in resolution provided by the IDM-DSM technique. The smallest periodicity in the sample ($p_y = 340$ nm) is below the Rayleigh resolution limit ($p_y < \lambda/(2NA_o) \sim 356$ nm; as such, observation of this periodicity when $NA_c = 0.97$, demonstrates the capability of IDM-DSM for imaging photonic crystals with $\lambda/(NA_o+NA_c) < p < \lambda/(2NA_o)$. This is in excellent correspondence with the predicted minimal observable period $p_y > \lambda/(NA_o+NA_c) \sim 322$ nm.

The heart of the FPM and DSM phase-recovery algorithms lies in the fact that an interference pattern is formed in the microscope's RP when a periodic structure is illuminated by a plane wave. Therefore, using Fourier optical considerations [12], the optical disturbance (complex electric field) at the microscope's FP is calculated in the FPM and DSM phase-recovery algorithms through a Fourier transformation of the optical disturbance at the sample's plane, and the optical disturbance in the microscope's RP plane is calculated through an inverse Fourier transformation of the optical disturbance at the microscope's FP [23-28]. Consequently, the use of the (IDM) FPM and DSM phase-recovery algorithms are only justified if interference of light diffracted by the sample through different optical paths occurs. However, diffraction of a plane wave by a periodic structure immersed in a medium with refractive index (n) only produces an interference pattern when $p > \lambda/(2n)$ [40]. This determines that the resolution limit of the high-resolution RP image numerically obtained using the IDM (ring-based) FPM and DSM phase-recovery algorithms only can be improved by increasing NA_c up to the maximum between $\lambda/(NA_o+NA_c)$ and $\lambda/(2n)$. Available optical-grade dielectric materials have $n < 2$; this resulting in $p_{\min} > 100$ nm.

The promise of imaging with plasmonics to overcome this $\lambda/(2n)$ limit is based on the fact that SPPs may have an effective refractive index $n \gg 2$

[37, 41]. This is in correspondence with the simulation results shown in Fig. 4, which were obtained using the commercial software package BandSolve™ from RSoft [42].

Fig. 4 shows the dispersion of the effective refractive index (n) of the SPPs excited in a plasmonic UTC with a structure like the one shown in the inset of Fig. 1e, but with a GaP substrate instead of glass. The more interesting feature of the dispersion relation plotted in Fig. 4 is that $n > 9$ for a vacuum wavelength ~ 570 nm. This results in a reduction of the resolution limit to $\lambda/(2n) \sim 32$ nm. Therefore, when the SPPs excited at the gold-GaP interface in the plasmonic UTCs are diffracted by a periodic structure with $p > 32$ nm at the sample's plane, the leakage radiation coupled to the diffracted SPPs should produce an interference pattern at the microscope's FP. This means, for instance, that using the microscope-UTC arrangement sketched in Fig. 1e with $NA_o = 1.5$, to image a plasmonic crystal structure (like the one shown in the inset of Fig. 1e) on a GaP substrate, with $p < \lambda/(2NA_o) \sim 190$ nm, can produce experimental FP-RP pairs of images like those shown in Figs. 1c and 1d, respectively. Like in Fig. 1d, no trace of the periodic structure of the plasmonic crystal would be visible in the low-resolution RP images formed directly in the camera. Similarly, like in Fig. 1c, the

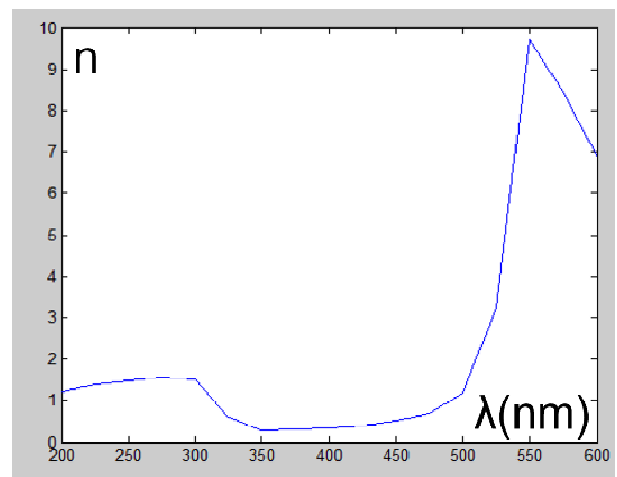


Fig. 4 Calculated dispersion of the effective refractive index (n) of the SPPs excited in a plasmonic UTC with a GaP substrate.

zero-order diffraction ring would not be visible in the FP image because $NA_o \ll NA_c = n \sim 9$ [29, 30]. However, arcs corresponding to the first-order diffraction rings may be visible. Despite that, when $p > \lambda/(NA_o+NA_c) \sim 54$ nm, using the IDM (ring-based) FPM and DSM phase-recovery algorithms should allow numerically obtaining a high-resolution RP image like the one shown in Fig. 1b where the periodic structure of the plasmonic crystal would be visible. We thus foresee that the microscope-UTC combination sketched in Fig. 1d should result in a novel optical nanoscope capable of imaging the intensity and phase of the electric field distribution, in the far-field, produced by nanostructures placed on the plasmonic UTC with a GaP substrate.

4. Conclusions

We discussed why it is not possible to directly obtain an image with a resolution better than the Rayleigh resolution limit in a camera. We also discussed how the use of a microscope-UTC arrangement with $NA_c > NA_o$, in combination with ring-based IDM FPM and DSM techniques allows for the numerical acquisition of a high-resolution image with increased resolution equal to the maximum value between $\lambda/(NA_o+NA_c)$ and $\lambda/(2n)$. Moreover, we presented simulation results suggesting that a plasmonic UTC with a transparent semiconductor substrate may have $n \gg 1$. Consequently, we argued that a combination of a common optical microscope, a plasmonic UTC with a semiconductor substrate, and a ring-based IDM phase-recovery algorithm should be capable of imaging the intensity and the phase of the electric field distribution produced by nanostructures placed on the plasmonic UTC, in the far-field.

References

- [1] Hetcht, E. 1998. *Optics*. Third Edition, Addison Wesley.
- [2] Born, M., and Wolf, E. 1975 *Principles of Optics*. 5th edition. Pergamon Press.
- [3] Hopkins, H. H., and Barham P. M. 1950. "The Influence of the Condenser on Microscopic Resolution." *Proceedings of the Physical Society* 63: 737.
- [4] Köheler, H. 1981. "On Abbe's Theory of Image Formation in the Microscope." *Optica Acta* 28: 1691.
- [5] Betzig, E., Isaacson, M., and Lewis, A. 1987. "Collection Mode near Field Scanning Optical Microscopy." *Appl. Phys. Lett.* 51: 2088-90.
- [6] Hell, S. W., and Krough, M. 1995. "Ground-State Depletion Fluorescence Microscopy, a Concept for Breaking the Diffraction Resolution Limit." *Appl. Phys. B* 60: 495-7.
- [7] Klar, T. A., Jakobs, S., Dyba, M., Egner, A., and Hell, S. W. 2000. "Fluorescence Microscopy with Diffraction Resolution Broken by Stimulated Emission." *PNAS* 97: 8206-10.
- [8] Zhuang, X. 2009. "Nano-Imaging with STORM." *Nature Photonics* 3: 365-7.
- [9] Gustafsson, M. G. 2000. "Surpassing the Lateral Resolution Limit by a Factor of Two Using Structured Illumination Microscopy." *J. Microsc.* 198: 82-7.
- [10] Chowdhury, S., Dhalla, A., and Isatt, J. 2012. "Structured Oblique Illumination Microscopy for Enhanced Resolution Imaging of Non-fluorescent, Coherently Scattering Samples." *Biomedical Opt. Express* 3: 1841-54.
- [11] Gustafsson, M. G. 2005. "Nonlinear Structured-Illumination Microscopy: Wide-Field Fluorescence Imaging with Theoretical Unlimited Resolution." *PNAS* 102: 13081-6.
- [12] Goodman, J. W. 1968. *Introduction to Fourier Optics*. McGraw-Hill.
- [13] Sayre, D. 1952. "Some Implications of a Theorem due to Shannon." *Acta Crystallogr.* 5: 843.
- [14] Gerchberg R. W., and Saxton, W. O. 1972. "A Practical Algorithm for Determination of Phase from Image and Diffraction Plane Pictures." *Optik* 35: 237-45.
- [15] Fienup, J. R. 1982. "Phase Retrieval Algorithms: A Comparison." *Appl. Opt.* 21: 2758-69.
- [16] Hillman, T. R., Gutzler, T., Alexandrov, S. A., and Sampson, D. D. 2009. "High-Resolution, Wide-Field Object Reconstruction with Synthetic Aperture Fourier Holographic Optical Microscopy." *Opt. Express* 17: 7873-92.
- [17] Tippie, A. E., Kumar, A., and Fienup, J. R. 2011. "High-Resolution Synthetic-Aperture Digital Holography with Digital Phase and Pupil Correction." *Opt. Express* 19: 12027-38.
- [18] Turpin, T., Gesell, L., Lapidés, J., and Price, C. 1995. "Theory of the Synthetic Aperture Microscope." *Proc. SPIE* 2566: 230-40.
- [19] Faulkner, H. M. L., and Rodenburg, J. M. 2004. "Movable Aperture Lensless Transmission Microscopy: A Novel Phase Retrieval Algorithm." *Phys. Rev. Lett.* 93: 023903.

- [20] Rodenburg, J. M., Hurst, A. C., Cullis, A. G., Dobson, B. R., Pfeiffer, F., Bunk, O., David, C., Jefimovs, K., and Johnson, I. 2007. "Hard-X-Ray Lensless Imaging of Extended Objects." *Phys. Rev. Lett.* 98: 034801.
- [21] Humphry, M., Kraus, B., Hurst, A., Maiden, A., and Rodenburg, J. 2012. "Ptychographic Electron Microscopy Using High-Angle Dark-Field Scattering for Sub-nanometre Resolution Imaging." *Nature Communications* 3: 730.
- [22] Maiden, A. M., Rodenburg, J. M., and Humphry, M. J. 2010. "Optical Ptychography: A Practical Implementation with Useful Resolution." *Opt. Lett.* 35: 2585-7.
- [23] Zheng, G., Horstmeyer, R., and Yang, C. 2013. "Wide-Field, High-Resolution Fourier Ptychographic Microscopy." *Nat. Photonics* 7: 739-45.
- [24] Ou, X., Horstmeyer, R., Zheng, G., and Yang, C. 2015. "High Numerical Aperture Fourier Ptychography: Principle, Implementation and characterization." *Opt. Express* 23: 3472-91.
- [25] Sen, S., Ishtiaque, A., Aljubran, B., Bernussi, A. A., and Grave de Peralta, L. 2016. "Fourier Ptychographic Microscopy Using an Infrared-Emitting Hemispherical Digital Condenser." *Appl. Optics* 55: 6421-7.
- [26] Ishtiaque, A., Alotaibi, M., Skinner-Ramos, S., Dominguez, D., Bernussi, A. A., and Grave de Peralta, L. 2017. "Fourier Ptychographic Microscopy at Communication Wavelengths Using a Femtosecond Laser." *Opt. Comm.* 405: 363-7.
- [27] Desai, D. B., Sen, S., Zhelyeznyakov, M. V., Alenazy, W., and Grave de Peralta, L. 2016. "Super-Resolution Imaging of Photonic Crystals Using Dual-Space Microscopy." *Appl. Opt.* 55: 3929-34.
- [28] Alotaibi, M., Gedies, R., Alzayed, A., Aldawsari, F., Dominguez, D., and Grave de Peralta, L. 2017. "Laser-Based Dual-Space Microscopy." *Opt. Comm.* 402: 662-7.
- [29] Desai, D. B., Dominguez, D., Bernussi, A. A., and Grave de Peralta, L. 2014. "Ultra-Thin Condensers for Optical Sub-wavelength Resolution Microscopy." *J. Appl. Phys.* 115: 093103.
- [30] Grave de Peralta, L. 2015. "Metal Slab Superlens-Negative Refractive Index versus Inclined Illumination: Discussion." *JOSA A* 32: 1729-35.
- [31] Dong, S., Shiradkar, R., Nanda, P., and Zheng, G. 2014. "Spectral Multiplexing and Coherent-State Decomposition in Fourier Ptychographic Imaging." *Biomed. Opt. Express* 5: 1758-67.
- [32] Tian, L., Li, X., Ramchandran, K., and Waller, L. 2014. "Multiplexed Coded Illumination for Fourier Ptychography with LED Array Microscope." *Biomed. Opt. Express* 14: 3093.
- [33] Alotaibi, M., Skinner-Ramos, S., Alamri, A., Alharbi, B., Alfarraj, M., and Grave de Peralta, L. 2017. "Illumination Direction Multiplexing Fourier Ptychographic Microscopy Using Hemispherical Digital Condensers." *Appl. Opt.* 56: 4052-7.
- [34] Frisbie, S. P., Chesnutt, C., Holtz, M. E., Krishnan, A., Grave de Peralta, L., and Bernussi, A. A. 2009. "Image Formation in wide-Field Microscopes Based on Leakage of Surface Plasmon-Coupled Fluorescence." *IEEE Photonics Journal* 1: 153-62.
- [35] Regan, C. J., Grave de Peralta, L., and Bernussi, A. A. 2012. "Equifrequency Curve Dispersion in Dielectric-Loaded Plasmonic Crystals." *Journal of Applied Physics* 111: 073105.
- [36] Gryczynski, I., Malicka, J., Gryczynski, Z., and Lakowicz, J. R. 2004. "Surface Plasmon-Coupled Emission with Gold Films." *J. Phys. Chem. B* 108: 12568-74.
- [37] Raether, H. 1988. *Surface Plasmons on Smooth and Rough Surfaces and on Gratings*. Berlin: Springer-Verlag.
- [38] Drezet, A., Hohenau, A., Koller, D., Stepanov, A., Ditzbacher, H., Steinberger, B., Aussenegg, F. R., Leitner, A., and Krenn, J. R. 2008. "Leakage Radiation Microscopy of Surface Plasmon Polaritons." *Materials Science and Engineering B* 149: 220.
- [39] Lopez-Boada, R., Regan, C. J., Dominguez, D., Bernussi, A. A., and Grave de Peralta, L. 2013. "Fundamentals of Optical Far-Field Subwavelength Resolution Based on Illumination with Surface Waves." *Opt. Express* 21: 11928-42.
- [40] Feynman, R. P., Leighton, R. B., and Sands, M. 1966. *The Feynman Lectures in Physics*. Addison Wesley, Vol. 3.
- [41] Ozbay, E. 2006. "Plasmonics: Merging Photonics and Electronics at Nanoscale Dimensions." *Science*, 311: 189-93.
- [42] RSoft Corporation, <http://www.rsoftdesign.com>.